Published in final edited form as:
J Immunol. 2012 April 1; 188(7): 3237–3246. doi:10.4049/jimmunol.1103065.

Actin reorganization is required for the formation of polarized BCR signalosomes in response to both soluble and membrane-associated antigens[1]

Chaohong Liu[*], **Heather Miller**[*], **Gregory Orlowski**[‡], **Haiyin Hang**[§], **Arpita Upadhyaya**[†], and **Wenxia Song**[*]

Wenxia Song: wenxsong@umd.edu

[*]Department of Cell Biology & Molecular Genetics, University of Maryland, College Park, MD 20742

[†]Department of Physics, University of Maryland, College Park, MD 20742

[‡]Department of Medicine, University of Massachusetts Medical School, Worchester, MA 01655

[§]National Laboratory of Biomacromolecules, Institute of Biophysics, Chinese Academy of Sciences, Beijing, China

Abstract

B-cells encounter both soluble (sAg) and membrane-associated antigens (mAg) in the secondary lymphoid tissue, yet how the physical form of Ag modulates B-cell activation remains unclear. This study compares actin reorganization and its role in BCR signalosome formation in mAg- and sAg-stimulated B-cells. Both mAg and sAg induce F-actin accumulation and actin polymerization at BCR microclusters and at the outer rim of BCR central clusters, but the kinetics and magnitude of F-actin accumulation in mAg-stimulated B-cells are greater than those in sAg-stimulated B-cells. Accordingly, the actin regulatory factors, cofilin and gelsolin, are recruited to BCR clusters in both mAg- and sAg-stimulated B-cells but with different kinetics and patterns of cellular redistribution. Inhibition of actin reorganization by stabilizing F-actin inhibits BCR clustering and tyrosine phosphorylation induced by both forms of Ag. Depolymerization of F-actin leads to unpolarized microclustering of BCRs and tyrosine phosphorylation in BCR microclusters without mAg and sAg, but in much slower kinetics than those induced by Ag. Therefore, actin reorganization, mediated via both polymerization and depolymerization, is required for the formation of BCR signalosomes in response to both mAg and sAg.

Introduction

Mature B-cells encounter their cognate antigen (Ag) when they circulate through the secondary lymphoid organs, where they are attracted into follicles through a CXCL13 gradient generated by follicular dendritic cells and fibroblastic reticular cells (1-3). The binding of Ag to the clonally specific B-cell receptor (BCR) initiates B-cell activation. In contrast to the T-cell receptor, the BCR can bind Ag in diverse forms. Two broad forms of Ag that B-cells commonly encounter in the secondary lymphoid organs are soluble (sAg) and membrane-associated Ag (mAg). Recent studies using multiphoton intravital

[1]This work was supported by a grant from National Institute of Health (AI059617 to WS), the Research and Scholarship Award by the Graduate School at University of Maryland (WS), and an Interdisciplinary and Engaged Research Seed Grant from NSF ADVANCE Program for Inclusive Excellence (WS).

Correspondence to: Wenxia Song, wenxsong@umd.edu.

microscopy have shown that sAg with relatively small molecular weight (≤60 kDa), when injected subcutaneously, rapidly reach B-cell follicles in the drainage lymph node, probably via gaps in the sinus floor (4) or the collagen-rich conduit network (5, 6). The conduits, which are secreted by fibroblastic reticular cells, passively deliver small molecules, like Ag and the B-cell chemokine CXCL13 (5, 6). Macrophages lining the lymph node subcapsular sinus capture and transport particulate Ag and immune complexes to follicles (7-9). Dendritic cells in the medullary sinus capture Ag and transport Ag to the B-cell compartment. Moreover, follicular dendritic cells can capture sAg in complexes with complement factors or antibody (Ab) and retain them for long term presentation (5, 10, 11). Ag captured by macrophages and dendritic cells is presented to B-cells in a membrane-associated form.

While *in vitro* B-cells readily bind both sAg and mAg, how B-cells are activated by different forms of Ag *in vivo* is not completely clear. Ag binding to the BCR can induce signaling cascades as well as Ag uptake, processing and presentation. The cellular activities triggered by BCR-Ag interaction and signals from the microenvironment of B-cells collectively determine the fate of B-cells. The activation of B-cells by both sAg and mAg has been studied extensively *in vitro* (12-16). Early studies, starting from the 1970s, mainly focused on sAg. These studies show that multivalent but not monovalent sAg induces the aggregation of surface BCRs into a central cluster at one pole of a B-cell, which was called a BCR cap (17-19). Later, Chen *et al.* (20) found that aggregated BCRs associated with lipid rafts, where Src kinases, such as Lyn, are constitutively present. The phosphorylation of the immunoreceptor tyrosine-based activation motifs in the cytoplasmic tails of the BCR by Src kinases leads to the activation of signaling cascades (15, 21). The requirement of multivalent sAg for BCR activation indicates the importance of Ag-induced BCR aggregation in BCR activation.

Recent studies utilizing total internal reflection fluorescence microscopy (TIRFM) provide high resolution live cell images of BCR signaling initiation events at the surface of B-cells interacting with Ag tethered to planar lipid bilayers. Ag tethered to lipid bilayers is a widely used model for mAg. The binding of mAg, even monovalent mAg, to the BCR induces conformational changes and self-aggregation of surface BCRs (22, 23). The newly formed BCR microclusters reside in lipid rafts (24) and recruit signaling molecules, including Lyn, Syk (23), PLCγ2, Vav (25) and co-stimulatory receptor CD19 (26). BCR microclusters increase in size over time by trapping more BCRs and eventually merge together to form a central cluster at the surface zone contacting Ag-tethered membrane, similar to the BCR cap. When the adhesion molecule ICAM is present on Ag-tethered membranes, the BCR central cluster is surrounded by ICAM, forming a surface macromolecular structure (SMAC) similar to the immunological synapse between T-cells and Ag presenting cells (27). Unlike T-cells, ICAM facilitates, but is not required for the formation of BCR signalosomes in response to mAg (27, 28).

Concurrent with BCR aggregation, mAg also induces B-cell spreading and contraction on the Ag tethered membrane (29). Such morphological changes have been shown to increase Ag gathering and BCR aggregation at the B-cell surface. B-cell morphological changes and amplified BCR aggregation are dependent on BCR signaling mediated by CD19, Btk, Vav and Rac2 (25, 26, 30), suggesting that BCR proximal signaling induced by mAg provides a positive feedback for the BCR signalosome formation. Similar to the B-cell response to mAg, morphological changes have been also observed in sAg-stimulated B-cells, where these B-cells form membrane protrusions in the vicinity of the BCR central cluster (19).

The actin cytoskeleton has been shown to be an important factor in B-cell activation (31). It was first observed more than thirty years ago that sAg induced F-actin accumulation at the

BCR cap (32-35). A link between the actin cytoskeleton and BCR signaling was first suggested by Baeker *et al*. who showed that disrupting the actin cytoskeleton by cytochalaisin D induced Ca^{2+} flux (36). Later studies reported that perturbation of the actin cytoskeleton delayed the attenuation of protein tyrosine phosphorylation (37) and enhanced activation of the MAP kinase, ERK, and the transcription factors, SRF, NF-κB and NFAT, induced by sAg (38). The underlying mechanism by which the actin cytoskeleton contributes to sAg-induced BCR activation remains to be elucidated. Recent studies using TIRFM show that the cortical actin network secured to the B-cell membrane by ezrin controls the lateral movement of surface BCRs (39, 40). Disrupting the cortical actin network inhibits surface BCR aggregation and B-cell spreading in response to mAg (29). However, in the absence of mAg, perturbation of cortical actin increases the lateral diffusion of surface BCRs and induces spontaneous signaling (39, 41). Our recent study demonstrates that the BCR proximal signaling molecule Btk and its negative regulator SH2-containing inositol-5 phosphatase-1 (SHIP-1) positively and negatively regulate actin reorganization induced by mAg, respectively. Btk activates actin nucleation promoting factor, Wiskott Aldrich symptom protein (WASP), promoting BCR aggregation and B-cell spreading (42, 43). In contrast, SHIP-1 inhibits the activation of Btk and WASP, promoting the contraction of B-cells and the merger of BCR microclusters into a central cluster (43). These data collectively reveal a critical role for the actin cytoskeleton in BCR activation induced by mAg. It remains unclear whether the actin cytoskeleton plays a similar role in sAg-induced BCR activation.

In this study, we compared the role of the actin cytoskeleton in BCR activation induced by sAg and mAg. Our results show that both mAg and sAg induce F-actin accumulation, actin polymerization, and the recruitment of the actin regulatory factors to BCR clusters, even though the kinetics and magnitude of these events are different in the two cases. Inhibition of actin reorganization by stabilizing F-actin blocks BCR clustering and tyrosine phosphorylation induced by both forms of Ag. Depolymerization of F-actin leads to unpolarized microclustering of BCRs and tyrosine phosphorylation in BCR microcluster without sAg and mAg. Our results demonstrate a similar role for the actin cytoskeleton in the initiation of BCR activation induced by mAg and sAg.

Materials and Methods

Mice and Cells

Mice (CBA/CaJ) (Jackson Laboratories, Bar Harbor, ME) of 6-12 weeks old were used. To purify splenic B-cells, mononuclear cells isolated using Ficoll density-gradient centrifugation (Sigma-Aldrich, St Louis, MO) were treated with anti-Thy1.2 mAb (BD Biosciences, San Jose, CA) and guinea pig complement (Rockland Immunobiochemicals, Gilbertsville, PA) to remove T-cells and panned for 1 h to remove monocytes and dendritic cells.

Model antigens

Alexa Fluor 546 conjugated mono-biotinylated Fab′-anti-mouse IgM+G antibody (AF546-mB-Fab′-anti-Ig) was used to label the BCR. It is generated from the $F(ab')_2$ fragment (Jackson ImmunoResearch, West Grove, PA) using a published protocol (44). To activate B-cells with soluble Ag (sAg), splenic B-cells were incubated with AF546-mB-Fab′-anti-Ig (2 μg/ml) mixed with mB-Fab′-anti-Ig (8 μg/ml) for 30 min and streptavidin (1 μg/ml) for 10 min at 4°C. As a control, streptavidin was omitted. The cells were washed and warmed up to 37°C for varying lengths of time. To activate B-cells with membrane-associated Ag (mAg), cells were incubated with AF546-mB-Fab′-anti-Ig and mB-Fab′-anti-Ig tethered to planar lipid bilayers by streptavidin at 37°C for varying lengths of time. As a control for mAg,

surface BCRs were labeled with AF546-Fab-anti-mouse IgM+G (2 μg/ml) at 4°C, washed, and then the B-cells were incubated with transferrin (Tf)-tethered lipid bilayers where the molecular density of Tf on lipid bilayers was equivalent to that of AF546-mB-Fab′-anti-Ig.

The planar lipid bilayer was prepared as described previously (24, 45). Briefly, liposomes were made by sonication of 1,2-Dioleoyl-sn-Glycero-3-phosphocholine and 1,2-Dioleoyl-sn-Glycero-3-phosphoethanolamine-cap-biotin (Avanti Polar Lipids, Alabaster, AL) in a 100:1 molar ratio in PBS at a lipid concentration of 5 mM. Aggregated liposomes were removed by ultracentrifugation and filtration. Coverslip chambers (Lab-Tek Nalge Nunc, Rochester, NY) were incubated with the liposomes (0.05 mM) for 10 min. After extensive washes, the coated coverslip chambers were incubated with 1 μg/ml streptavidin (Jackson ImmunoResearch), followed by 2 μg/ml AF546-mB-Fab′-anti-Ig mixed with 8 μg/ml mB-Fab′-anti-Ig antibody or 16 μg/ml biotin-Tf.

Confocal fluorescence microscopy and image analysis

Splenic B-cells were incubated with mAg or sAg at 37°C for varying lengths of time. The cells were fixed with 4% paraformaldehyde (PFA), permeabilized with 0.05% saponin, and stained with anti-cofilin, phosphorylated cofilin, gelsolin (Santa Cruz Biotechnology, CA), or phosphotyrosine (4G10, Millipore, Billerica, Massachusetts) antibodies. F-actin was stained with AF488-phalloidin (Invitrogen) or total actin by anti-actin antibody (Sigma, St. Louis, MO). Cells were analyzed using a confocal microscope (Zeiss LSM 710, Carl Zeiss Microscopy, Thornwood, NY). Series of Z-sections were acquired at 0.4 μm per section and reconstituted into 3-D using Zen software from Zeiss. The 2.5 D images, which show fluorescence intensity profiles of F-actin, cofilin, gelsolin or phosphotyrosine in relation to the BCR staining, were generated using Zen software. Pearson correlation coefficients between different staining were determined using LSM 510 software (46).

The ratio of fluorescence intensity at the cell pole of BCR aggregation to that at the opposite pole of the cells was determined using z-series of images and Andor iQ software (Andor Technology, Belfast, UK). For mAg-stimulated B-cells, the fluorescence intensity sum of three z-sections close to lipid bilayers and that at the top of the cell were determined. For sAg-stimulated B-cells, only B-cells with the BCR central cluster located at the top of the cells were selected for the analysis. The fluorescence intensity sum of three z-sections close to the BCR central cluster and that close to the coverslip were determined. The level of tyrosine phosphorylation in individual mAg-stimulated B-cells was determined by adding up the fluorescence intensity of phosphotyrosine staining in all z-sections of a cells using Andor iQ software. For each time point, the average fluorescence intensity was generated from ~50 individual cells from two or three independent experiments.

Total internal reflection microcopy and image analysis

Images were acquired using a Nikon laser TIRF system on an inverted microscope (Nikon TE2000-PFS), equipped with a 60X, 1.49 NA Apochromat TIRF objective (Nikon Instruments Inc., Melville, NY), a Coolsnap HQ2 CCD camera (Roper Scientific, Sarasota, FL), and two solid-state lasers of wavelength 491 nm and 561 nm. For live cell imaging, time lapse images were acquired at the rate of one frame every 3 sec. Image acquisition started upon the addition of B-cells onto Ag-tethered lipid bilayer and continued for 5 to 10 min at 37°C. Interference reflection microscopy (IRM) images and fluorescence images at 491 nm excitation (for AF488) and 561 nm excitation (for AF546) were acquired sequentially.

To image intracellular molecules, B-cells were incubated with mAg at 37°C for varying lengths of time, and then fixed with 4% PFA, permeabilized with 0.05% saponin, and

stained for cofilin, gelsolin, phosphotyrosine, and F-actin as described above. The B-cell contact area was determined using IRM images and MATLAB software (The MathWorks, Inc., Natick, MA). The total fluorescence intensity (TFI) of each staining in the B-cell contact zone was determined using Andor iQ software. Background fluorescence generated by Ag tethered to lipid bilayers in the absence of B-cells or secondary antibody controls was subtracted. For each set of data, more than 20 individual cells from two or three independent experiments were analyzed.

Analysis of actin nucleation sites

Actin nucleation sites were labeled as previously described (47). For B-cells that were incubated with sAg, cells were treated with 0.45 μM AF488-G-actin (Invitrogen) in the presence of 0.025% saponin during the last minute of incubation. For B-cells that were activated by mAg, B-cells were incubated with mAg in the presence of AF488-G-actin and 0.025% saponin for 5 min at 37°C. The cells were fixed and analyzed using Zeiss 710 confocal microscope to generate 3-D images and/or TIRFM.

Treatment of latrunculin B and Jasplakinolide

B-cells were pretreated with latrunculin B (Lat, 10 μM) or Jasplakinolide (Jas, 2 μM) (Calbiochem, Gibbstown, NJ) for 30 min at 37°C before the incubation with Ag in the presence of Lat or Jas. When B-cells were treated with Lat alone, the time course started at the addition of Lat.

Flow cytometry analysis

The tyrosine phosphorylation levels of sAg-stimulated B-cells were determined using flow cytometry. B-cells were incubated with sAg, Lat, or Jas plus sAg for varying lengths of time at 37°C. Then cells were fixed by 4% PFA, permeabilized by 0.05% saponin, and stained with anti-phosphotyrosine mAb. After post-fix with 2% PFA, the cells were analyzed using BD Canto II flow cytometer.

Statistical Analysis

Statistical significance was assessed by the Mann-Whitney test using Prism software (GraphPad Software, San Diego, CA).

Results

Both soluble and membrane-associated antigens induce the recruitment of F-actin to BCR aggregates

To compare actin reorganization induced by mAg and sAg, we chose a pseudo Ag system that can be applied as both soluble and membrane-associated forms. Alexa Fluor 546-conjugated, mono-biotinylated Fab′ fragment of goat-anti-mouse IgG+M (AF546-mB-Fab′-anti-Ig) was used to label surface BCRs. Labeled BCRs were aggregated either with soluble streptavidin (sAg) or streptavidin tethered onto lipid bilayers (mAg). The reorganization of the actin cytoskeleton and surface BCRs in B-cells stimulated with sAg was examined using 3-dimentional (3-D) confocal fluorescence microscopy (CFM) and those in B-cells stimulated with mAg using both 3-D CFM and total internal reflection fluorescence microscopy (TIRFM). The surface area of the cell in contact with Ag-tethered lipid bilayer (B-cell contact zone) was visualized by interference reflection microscopy (IRM). Upon incubation with mAg- but not with transferrin (Tf)-tethered lipid bilayers, surface BCRs on splenic B-cells aggregated into small clusters (3 min) and then formed a centralized cluster (7 min) at the B-cell contact zone. This was concurrent with a rapid increase of the B-cell contact zone in the early stages (1-6 min) and subsequent decrease (7 min) (Fig. 1A-C).

During BCR aggregation, the actin cytoskeleton underwent a dramatic redistribution, from a uniform distribution at the periphery of unstimulated cells to accumulation at the contact zone (Fig. 1A-C). By 7 min, the actin cytoskeleton was primarily concentrated at the outer edge of centralized BCR clusters and did not colocalize with BCR clusters extensively (Fig. 1A-B and 1E). In B-cells stimulated with sAg, surface BCRs also formed microclusters at 3 min and then a polarized central cluster at 7 min (Fig. 1D), which was similar to what was seen in mAg-stimulated B-cells. However, BCR clusters induced by sAg appeared less dense than those induced by mAg (Fig. 1A and 1D, bottom panels). Soluble Ag also induced the recruitment of F-actin to BCR clusters. F-actin accumulated not only at the periphery but also at the center of the BCR central cluster (Fig. 1D), colocalizing with the BCR extensively (Fig. 1E). In order to compare the kinetics and magnitude of actin redistribution in mAg- and sAg-stimulated cells, the ratio of F-actin fluorescence intensity in the CFM image slices at the BCR central cluster to that at the opposite pole of the BCR central cluster was determined. The two pole ratio of F-actin was about 1 in unstimulated B-cells that interacted with polylysine-coated glass or Tf-tethered lipid bilayers, and it increased over time in both mAg- and sAg-stimulated B-cells (Fig. 1F). This indicates a redistribution of F-actin from unpolarized to polarized distribution towards BCR clusters. The two pole ratio in mAg-stimulated B-cells increased faster and was two fold higher than that in sAg-stimulated B-cells at all the tested time points (Fig. 1F). Taken together, these results indicate that both mAg and sAg induce the recruitment of the actin cytoskeleton to BCR clusters along with BCR aggregation. Membrane-associated Ag appears to induce a greater degree of polarized actin redistribution than sAg.

Both soluble and membrane-associated antigens induce actin polymerization at BCR aggregates

The actin cytoskeleton is reorganized by rapid polymerization and depolymerization. To further compare actin remodeling induced by mAg with that induced by sAg, we analyzed the cellular distribution of *de novo* actin polymerization sites in relation to surface BCRs. Actin polymerization sites were detected by the incorporation of AF488-G-actin into polymerizing ends of actin filaments. AF488-G-actin was introduced into cells in the presence of a low concentration of non-ionic detergent during the last minute of incubation with sAg or during the entire incubation time with mAg. Intracellular incorporation of AF488-G-actin was significantly increased in splenic B-cells stimulated by mAg compared to B-cells incubated with Tf-tethered lipid bilayer (Fig. 2A). Both 3-D CFM (Fig. 2A) and TIRFM (Fig. 2B) analysis showed that actin polymerization sites were preferentially located at the outer edge of BCR clusters after a 5 min-incubation with mAg. Similarly, actin polymerization was undetectable in the absence of sAg (Fig. 2C, top panels). After sAg stimulation, *de novo* actin polymerization sites were first colocalized with BCR microclusters and later were exclusively found at the outer rim of BCR central clusters as they formed (Fig. 2C). These results show that both sAg and mAg induce actin polymerization, and that actin polymerization occurs at BCR microclusters and at the outer edge of the BCR central cluster.

Both soluble and membrane-associated antigens induce the mobilization of actin regulators, cofilin and gelsolin

Actin reorganization induced by Ag indicates that antigenic stimulation triggers the activation of actin regulators. Our previous studies have demonstrated that both mAg and sAg can induce Btk-dependent activation of WASP, an actin nucleation promoting factor (42, 43). Here we compared the effects of mAg and sAg on the cellular redistribution of actin regulators, cofilin and gelsolin. Cofilin can either stabilize or destabilize F-actin depending on its concentration in the cytoplasm, and its F-actin binding activity is inhibited by phosphorylation (48). Gelsolin severs F-actin in a calcium dependent manner (49). The

cellular distribution of cofilin and gelsolin in splenic B-cells was analyzed using specific antibodies. In the control conditions where splenic B-cells interact with Tf-tethered lipid bilayers (Fig. 3A, top panels) or with polylysine-coated glass slides (Fig. 3B, top panels), cofilin distributed evenly at the cell periphery. Reconstituted 3-D CFM images showed that in mAg-stimulated B-cells, cofilin was recruited to BCR clusters as early as 3 min, surrounding the BCR central cluster (Fig. 3A). However, TIRFM did not detect a significant amount of cofilin at the B-cell contact zone (Fig. 3C), suggesting that recruited cofilin does not associate with the plasma membrane and is at least 200 nm away from the contact zone. Reconstituted 3-D CFM images showed that cofilin was primarily located at the top of the BCR central cluster (Fig. 3A, bottom panels). In sAg-stimulated splenic B-cells, cofilin was clearly recruited to BCR aggregates at early times and the central clusters at later times (Fig. 3B). Reconstituted 3-D images and 2.5-D fluorescence intensity profiles showed extensive colocalization of cofilin with the BCR central cluster (Fig. 3B and 3D), distinct from the distribution of cofilin in mAg-stimulated B-cells (Fig. 3A and 3D). The colocalization of cofilin with the BCR in sAg-stimulated B-cells, as quantified by Pearson's correlation coefficients, increased over time for 10 min and decreased by 30 min as the BCR was internalized (Fig. 3E).

To determine whether cofilin recruitment is dependent on signaling, B-cells were pretreated with the Src kinase inhibitor PP2. This treatment inhibited BCR central cluster formation and reduced the colocalization of cofilin with the BCR to basal levels in sAg-stimulated B-cells (Fig. 3E and 3G). To determine whether the cofilin recruited to BCR clusters is activated, we stained for phosphorylated cofilin (p-cofilin) which is incapable of binding to F-actin (50). In mAg-stimulated B-cells, p-cofilin was recruited neither to the B-cell contact zone (Fig. 3F) nor to the region above the contact zone (Fig. 3H) in comparison with B-cells interacting with Tf tethered lipid bilayers. In sAg-stimulated B-cells, p-cofilin was largely excluded from BCR clusters (Fig. 3I) and did not colocalize with the BCR (Fig. 3J). The differential distribution of total cofilin and p-cofilin suggests that most of cofilin that co-clustered with surface BCRs is active. Similar to F-actin recruitment, the fluorescence intensity ratio of cofilin at the BCR central cluster to that at the opposite pole increased over time in both mAg- and sAg-stimulated B-cells, but it increased much faster and reached higher levels in mAg-stimulated cells than in sAg-stimulated cells (Fig. 3K).

Incubation of splenic B-cells with either mAg or sAg led to the redistribution of gelsolin to BCR clusters in splenic B-cells, where gelsolin staining appeared punctate (Fig. 4A and 4C). Similar to cofilin, gelsolin surrounded the BCR central cluster in mAg-stimulated B-cells (Fig. 4A), but colocalized with the BCR through the central cluster in sAg-stimulated B-cells (Fig. 4C-D). There was no significant amount of gelsolin detected in the contact zone of mAg-stimulated B-cells by TIRFM (Fig. 4B). The Pearson's correlation coefficients showed a similar increase in the colocalization of gelsolin with the BCR over time as for cofilin (Fig. 4E). The two pole ratio of gelsolin fluorescence intensity increased over time and was much higher (~4 fold) in mAg-stimulated cells than that in sAg-stimulated cells (Fig. 4F).

Taken together, these results show that both mAg and sAg induce the recruitment of cofilin and gelsolin to BCR clusters; however their recruitment kinetics and magnitude and their distribution are different in mAg- and sAg-stimulated B-cells.

Disruption of the actin cytoskeleton alters BCR activation in response to both soluble and membrane-associated antigens as well as antigen-independent BCR signaling

To compare the role of the actin cytoskeleton in BCR activation induced by mAg and sAg, we disrupted the actin cytoskeleton utilizing a pharmacological approach using latrunculin B (Lat) and jasplakinolide (Jas). Lat promotes actin depolymerization by sequestering G-actin

(51), while Jas stabilizes F-actin and binds F-actin at the same site as phalloidin (52). We used these two reagents at concentrations that abolished most phalloidin staining (Fig. S1), which indicates that Lat depolymerizes and Jas binds most F-actin in B-cells at these concentrations. Using both 3-D CFM and TIRFM, we found that at these concentrations, both the pretreatment of Lat and Jas dramatically reduced BCR aggregation at the B-cell contact zone (Fig. 5A-B and Fig. 6A-C) as well as B-cell spreading on Ag-tethered lipid bilayers (Fig. 5A and 5C) (Supplemental Video 1). Similarly, Jas pretreatment inhibited the formation of BCR clusters induced by sAg (Fig. 6F-H). These data indicate that BCR aggregation induced by both mAg and sAg requires actin reorganization.

In order to investigate whether the effect of Jas and Lat on BCR aggregation has any impact on BCR signaling, we examined the distribution and level of tyrosine phosphorylation (pY) using phosphotyrosine mAb by both microscopy and flow cytometry approaches. The staining of pY was detected at BCR clusters in response to both mAg and sAg, but appeared in distinct distribution patterns with relation to the BCR central cluster (Fig. 6A-B and 6F-G). It was primarily located at the outer edge of the BCR central cluster in mAg-stimulated B-cells (Fig. 6B, 6E, and 6J), but colocalized extensively with the BCR throughout the central cluster in sAg-stimulated B-cells (Fig. 6G and 6J). The pY levels in splenic B-cells dramatically increased in response to both mAg and sAg, peaking at ~2 min and returning to the basal level by 10 min (Fig. 6K-L). Pretreatment with Jas blocked tyrosine phosphorylation induced by both mAg and sAg (Fig. 6C, 6H, and 6K-L).

The actin cytoskeleton has been shown to regulate Ag-independent signaling in B-cells by controlling BCR lateral mobility (39). To understand how actin is involved in signaling regulation in resting B-cells, we determined the effect of Lat and Jas at the concentrations that eliminate or bind most F-actin (Fig. S1) on BCR aggregation and tyrosine phosphorylation in unstimulated B-cells attached to lipid bilayers by Tf or attached to polylysine-coated glass slides. The reconstituted 3-D CFM analysis showed that when B-cells were treated with Lat in the absence of Ag, surface BCRs formed microclusters in a non-polarized manner (Fig. 6D and 6I). There were very few BCR microclusters detected by TIRFM in the B-cell membrane zone contacting Tf-tethered lipid bilayers (Fig. 6E, bottom panels). BCR microclusters in Lat-treated cells formed at 10 min, which is later than those induced by mAg and sAg (data not shown), and remained randomly distributed at 30 min (Fig. 6D and 6I). These BCR microclusters were positive for pY staining (Fig. 6D and 6I), suggesting that tyrosine phosphorylation occurs at these microclusters. Quantitative analysis showed that Lat treatment alone increased the pY level in unstimulated B-cells. However, this Lat-induced pY increase had much slower kinetics than that induced by Ag and did not show any sign of attenuation for at least 30 min (Fig. 6K-L). In contrast, Jas treatment induced neither BCR aggregation nor tyrosine phosphorylation (data not shown).

These results collectively suggest that actin depolymerization itself is sufficient for BCR self-aggregation into microclusters and signal induction in BCR aggregates; however actin polymerization may be essential for the fast kinetics of BCR aggregation and signal activation and the merger of BCR microclusters into the central cluster as well as signaling attenuation induced by both mAg and sAg.

Discussion

Two of the common physical forms of Ags that B-cells encounter in the draining lymph node and spleen are soluble Ag and Ag presented on the surface of dendritic cells and macrophages (3). How the physical presentation of Ag modulates BCR signaling has not been well studied. Previous studies have shown a role for the actin cytoskeleton in mAg-induced BCR activation (31). This study reveals that actin reorganization is equally

important for BCR signaling triggered by sAg. Both mAg and sAg induce actin reorganization and recruitment of actin regulators to BCR aggregates. Inhibition of actin reorganization by stabilizing F-actin blocks BCR aggregation and tyrosine phosphorylation induced by both mAg and sAg. Elimination of most F-actin by depolymerization leads to the unpolarized formation of BCR microclusters and tyrosine phosphorylation in the BCR microcluster in the absence of Ag. These data indicate an essential role for the actin cytoskeleton in BCR activation, irrespective of the nature of Ag presentation.

Because of their different physical forms, sAg and mAg have distinct modes of interaction with surface BCRs. While sAg can bind BCRs on the entire surface of B-cells at the same time in a non-polarized fashion, mAg can only bind BCRs at the surface zone contacting the Ag-tethered membrane, which provides a polarized stimulation. Although both sAg and mAg can induce BCR self-aggregation into microclusters and central clusters by cross-linking BCRs, They do so in distinct ways. Upon sAg stimulation, surface BCRs have to identify a pole of the cell to laterally migrate towards in order to form the BCR central cluster. Further, mAg induces more dramatic morphological changes in B-cells than sAg. These observations suggest that the actin cytoskeleton plays distinct roles in mAg- and sAg-stimulated BCR activation. This study shows that while both mAg and sAg induce actin reorganization in splenic B-cells, the magnitude of F-actin and actin regulator recruitment in mAg-stimulated cells is generally greater than that in sAg-stimulated cells, as revealed by comparing the fluorescence intensity ratio between the pole where the BCR central cluster forms and its opposite pole. In addition, mAg-induce BCR redistribution appears to lead to the formation of a more compact BCR central cluster than sAg. Because we formulated mAg and sAg using the same reagents with the same concentrations and examined both using the same approach, the observed differences suggest that the physical form of Ag has an impact on actin reorganization and surface BCR aggregation, and mAg appears to be more potent in triggering these events compared to sAg.

In addition to differences in the recruitment levels, the distribution patterns of F-actin, cofilin and gelsolin are distinct in mAg- and sAg-stimulated B-cells. F-actin, cofilin and gelsolin are preferentially localized at the outer edge of the contact zone in mAg-stimulated B-cells, but are colocalized with the BCR throughout the central cluster in sAg-stimulated B-cells. Their differential distribution is likely linked to the distinct mechanisms by which BCR aggregates grow and merge with each other in mAg- and sAg-stimulated cells. After initial contacting with mAg, B-cells undergo rapid spreading on Ag-tethered membrane, which is followed by contraction (29). B-cell spreading has been shown to enhance BCR self-aggregation by allowing more surface BCRs to engage Ag, and B-cell contraction after spreading facilitates the merger of small BCR aggregates into the central cluster (29, 43). The co-accumulation of WASP, cofilin and gelsolin with F-actin at the outer edge of the contact membrane suggests that actin polymerization (by WASP), severing and/or depolymerization (by cofilin and gelsolin) occur at the leading edge of the spreading membrane, driving it outwards. This study also finds that in contrast to WASP (43), cofilin and gelsolin are not concentrated in the B-cell contact zone, but localized more than 200 nm above the BCR central cluster. This indicates that F-actin severing mediated by cofilin and gelsolin occurs above the BCR central cluster, which potentially promotes actin depolymerization at the cytoplasmic side of the actin cytoskeleton and provides G-actin monomers for WASP-mediated actin polymerization at the B-cell contact zone. Such a coordination of cofilin and gelsolin with WASP and other actin regulators potentially leads to actin reorganization in a unique manner that generates both a lateral force for B-cell spreading and contraction and a force that allows sustained adhesion of B-cells to Ag-tethered membrane. A recent study by Freeman *et al.* (53) shows that Rap GTPase-dependent activation of cofilin leads to actin severing, which is required for efficient B-cell

spreading and BCR aggregation, confirming a role for cofilin in BCR activation in response to mAg.

In contrast to mAg-stimulated B-cells, sAg-stimulated B-cells lack a target surface to adhere to and do not undergo dramatic morphological changes. The persistent colocalization of F-actin, cofilin and gelsolin with surface BCR aggregates in sAg-stimulated B-cells provides two hypotheses. First, the lateral movement of BCR aggregates and the dynamics of the actin cytoskeleton are functionally linked with each other. Second, both WASP activated actin polymerization and cofilin- and gelsolin-mediated actin severing and/or depolymerization occur at the plasma membrane, which potentially induces lateral mobilization of actin filaments to drive the later movement of BCRs but not the formation of lamellipodia for B-cell spreading. Further studies are required to test these hypotheses.

The differences in distribution of F-actin and actin regulators in mAg- and sAg-stimulated B-cells raise the question of how these two types of Ags induce distinct modes of actin reorganization. Ag-triggered actin reorganization has been shown to depend on BCR signaling. We have recently shown that the recruitment and activation of WASP are positively and negatively regulated by Btk and SHIP-1 respectively (42, 43). This study shows that cofilin and gelsolin, two actin regulators involved in actin severing and depolymerization, also co-clustered with surface BCRs in response to both mAg and sAg. Furthermore, the co-clustered cofilin is primarily in the unphosphorylated active form, which is capable of binding F-actin, and the co-clustering of cofilin with BCRs depends on BCR signaling. Freeman *et al.* (53) have recently shown that in B-cells cofilin is activated in a Rap GTPase-dependent manner in response to Ag stimulation. Gelsolin is known to be activated by calcium flux (54). The activity of cofilin has been shown to be regulated via a growing number of cellular pathways, including its phosphorylation and dephosphorylation by LIM kinases and phosphatases chronophin and slingshot 1L, its binding to phosphatidylinositides, and its local concentration relative to F-actin levels (55). These collectively indicate that the activation and recruitment of cofilin and gelsolin provide an additional level of control for BCR signaling to regulate actin reorganization. The physical presentation of Ags may regulate the spatiotemporal organization of BCR signalosomes, consequently leading to differential activation or distribution of these actin regulators.

How the physical presentation of Ag, soluble and membrane bound, impacts the initiation event of BCR signaling remains to be addressed. Association with the membrane transforms Ag stimulation from a non-polarized into a polarized one and potentially generates physical restraint on the Ag-BCR interaction. This increased physical restraint potentially enhances the ability of Ag to induce conformational changes in the BCR through putative mechanical feedback, thereby facilitating BCR self-aggregation. Tolar *et al.* (22) showed that a mono-valent Ag, which cannot induce BCR activation as a soluble form, induced BCR aggregation and signaling when it was tethered to lipid bilayers. This mono-valent mAg induces BCR self-aggregation probably by inducing conformational changes of the BCR, exposing the Cμ4 domain of membrane IgM that has been shown to be involved in BCR self-aggregation. Therefore, the physical form of Ag potentially modulates BCR activation via their ability to induce conformational change. This study shows that the phosphotyrosine stain has a different distribution pattern in mAg- as compared to sAg-stimulated B-cells. The pY staining is concentrated at the outer edge of the central cluster in mAg-stimulated B-cells, but is present throughout the central cluster in sAg-stimulated B-cells. This result suggests that mAg- and sAg-induced signalosomes differ in their spatial organization. Our finding that the distribution pattern of phosphotyrosine staining in mAg- and sAg-stimulated cells are similar to those of F-actin and actin regulators, cofilin and gelsolin supports the notion that differential actin remodeling contributes to the distinct spatial organization of BCR signalosomes in mAg- and sAg-stimulated B-cells.

Actin reorganization has been shown to be involved in the initiation of BCR signaling and the regulation of tonic signaling in resting B-cells (31, 39-41). How actin dynamics regulate BCR signaling at different activation stages in response to different forms of Ag remains to be elucidated. Similar to previous findings (29, 39), this study found that elimination of most F-actin by Lat induced tyrosine phosphorylation in the absence of Ag. Our study further shows that actin depolymerization by Lat induces BCR aggregation and that the BCR aggregates are positive for tyrosine phosphorylation. This suggests that actin depolymerization alone is sufficient for the induction of BCR aggregation and BCR aggregation is able to initiate BCR signaling. Additionally, our study found two distinct properties of Lat-induced BCR aggregates. First, Lat-induced BCR aggregation is slow, random and unpolarized compared to BCR aggregates induced by mAg and sAg, which is concurrent with a slow increase in tyrosine phosphorylation. Second, Lat-induced BCR aggregates persist as microclusters and are unable to merge into a polarized central cluster, which is associated with a lack of attenuation of Lat-induced tyrosine phosphorylation. The second property of Lat-induced BCR aggregates is similar to what we previously found in SHIP-1-deficient B-cells where BCR aggregates persist as microclusters and signaling attenuation is inhibited (43). This finding further supports the notion that the merger of BCR microclusters into the central cluster is associated with signal attenuation. These results collectively suggest that while actin depolymerization can induce BCR aggregation and BCR signaling, actin polymerization, in coordination with actin depolymerization, is important for the fast kinetics of BCR aggregation and activation as well as the merger of BCR aggregates into a central cluster and signaling attenuation.

Our studies demonstrate that actin remodeling is required for BCR activation in response to both mAg and sAg. In both cases, actin remodeling, including both polymerization and depolymerization, is essential for early and rapid BCR aggregation and the later growth and merger of these aggregates into a polarized central cluster. Actin remodeling induced by sAg and mAg exhibits different magnitude and spatial organization, which provides distinct feedback for the formation of BCR signalosomes. Future studies are required to define the molecular detail underlying the functional interaction between the actin cytoskeleton and BCR signaling during B-cell activation.

Supplementary Material

Refer to Web version on PubMed Central for supplementary material.

Acknowledgments

We thank Drs. Hae Won Sohn and Wanli Liu at Laboratory of Immunogentics, the National Institute of Allergy and Infectious Diseases, National Institutes of Health, for technical assistance on generating lipid bilayers. We thank Mr. King Lam Hui and Mr. Brian Grooman on technical assistance with TIRFM data analysis. We thank Mr. Ken Class, Ms. Amy Beaven, the Imaging Core and the Flow Cytometry Core Facility at University of Maryland for technical assistance.

References

1. Cyster JG, Ansel KM, Reif K, Ekland EH, Hyman PL, Tang HL, Luther SA, Ngo VN. Follicular stromal cells and lymphocyte homing to follicles. Immunol Rev. 2000; 176:181–193. [PubMed: 11043777]
2. Gunn MD, Ngo VN, Ansel KM, Ekland EH, Cyster JG, Williams LT. A B-cell-homing chemokine made in lymphoid follicles activates Burkitt's lymphoma receptor-1. Nature. 1998; 391:799–803. [PubMed: 9486651]
3. Gonzalez SF, Degn SE, Pitcher LA, Woodruff M, Heesters BA, Carroll MC. Trafficking of B cell antigen in lymph nodes. Annu Rev Immunol. 2011; 29:215–233. [PubMed: 21219172]

4. Pape KA, Catron DM, Itano AA, Jenkins MK. The humoral immune response is initiated in lymph nodes by B cells that acquire soluble antigen directly in the follicles. Immunity. 2007; 26:491–502. [PubMed: 17379546]
5. Bajenoff M, Germain RN. B-cell follicle development remodels the conduit system and allows soluble antigen delivery to follicular dendritic cells. Blood. 2009; 114:4989–4997. [PubMed: 19713459]
6. Roozendaal R, Mempel TR, Pitcher LA, Gonzalez SF, Verschoor A, Mebius RE, von Andrian UH, Carroll MC. Conduits mediate transport of low-molecular-weight antigen to lymph node follicles. Immunity. 2009; 30:264–276. [PubMed: 19185517]
7. Junt T, Moseman EA, Iannacone M, Massberg S, Lang PA, Boes M, Fink K, Henrickson SE, Shayakhmetov DM, Di Paolo NC, van Rooijen N, Mempel TR, Whelan SP, von Andrian UH. Subcapsular sinus macrophages in lymph nodes clear lymph-borne viruses and present them to antiviral B cells. Nature. 2007; 450:110–114. [PubMed: 17934446]
8. Phan TG, Green JA, Gray EE, Xu Y, Cyster JG. Immune complex relay by subcapsular sinus macrophages and noncognate B cells drives antibody affinity maturation. Nat Immunol. 2009; 10:786–793. [PubMed: 19503106]
9. Phan TG, Gray EE, Cyster JG. The microanatomy of B cell activation. Curr Opin Immunol. 2009; 21:258–265. [PubMed: 19481917]
10. Suzuki K, Grigorova I, Phan TG, Kelly LM, Cyster JG. Visualizing B cell capture of cognate antigen from follicular dendritic cells. J Exp Med. 2009; 206:1485–1493. [PubMed: 19506051]
11. Szakal AK, Kosco MH, Tew JG. A novel in vivo follicular dendritic cell-dependent iccosome-mediated mechanism for delivery of antigen to antigen-processing cells. J Immunol. 1988; 140:341–353. [PubMed: 3257233]
12. Harwood NE, Batista FD. Early events in B cell activation. Annu Rev Immunol. 2010; 28:185–210. [PubMed: 20192804]
13. Harwood NE, Batista FD. Visualizing the molecular and cellular events underlying the initiation of B-cell activation. Curr Top Microbiol Immunol. 2009; 334:153–177. [PubMed: 19521685]
14. Tolar P, Sohn HW, Pierce SK. Viewing the antigen-induced initiation of B-cell activation in living cells. Immunol Rev. 2008; 221:64–76. [PubMed: 18275475]
15. Dal Porto JM, Gauld SB, Merrell KT, Mills D, Pugh-Bernard AE, Cambier J. B cell antigen receptor signaling 101. Mol Immunol. 2004; 41:599–613. [PubMed: 15219998]
16. Kurosaki T, Shinohara H, Baba Y. B cell signaling and fate decision. Annu Rev Immunol. 2010; 28:21–55. [PubMed: 19827951]
17. Schreiner GF, Unanue ER. Membrane and cytoplasmic changes in B lymphocytes induced by ligand-surface immunoglobulin interaction. Adv Immunol. 1976; 24:37–165. [PubMed: 798475]
18. Schreiner GF, Unanue ER. Capping and the lymphocyte: models for membrane reorganization. J Immunol. 1977; 119:1549–1551. [PubMed: 334966]
19. Unanue ER, Perkins WD, Karnovsky MJ. Ligand-induced movement of lymphocyte membrane macromolecules. I. Analysis by immunofluorescence and ultrastructural radioautography. J Exp Med. 1972; 136:885–906. [PubMed: 4626851]
20. Cheng PC, Dykstra ML, Mitchell RN, Pierce SK. A role for lipid rafts in B cell antigen receptor signaling and antigen targeting. J Exp Med. 1999; 190:1549–1560. [PubMed: 10587346]
21. Kurosaki T. Functional dissection of BCR signaling pathways. Curr Opin Immunol. 2000; 12:276–281. [PubMed: 10781408]
22. Tolar P, Hanna J, Krueger PD, Pierce SK. The constant region of the membrane immunoglobulin mediates B cell-receptor clustering and signaling in response to membrane antigens. Immunity. 2009; 30:44–55. [PubMed: 19135393]
23. Tolar P, Sohn HW, Pierce SK. The initiation of antigen-induced B cell antigen receptor signaling viewed in living cells by fluorescence resonance energy transfer. Nat Immunol. 2005; 6:1168–1176. [PubMed: 16200067]
24. Sohn HW, Tolar P, Pierce SK. Membrane heterogeneities in the formation of B cell receptor-Lyn kinase microclusters and the immune synapse. J Cell Biol. 2008; 182:367–379. [PubMed: 18644892]

25. Weber M, Treanor B, Depoil D, Shinohara H, Harwood NE, Hikida M, Kurosaki T, Batista FD. Phospholipase C-gamma2 and Vav cooperate within signaling microclusters to propagate B cell spreading in response to membrane-bound antigen. J Exp Med. 2008; 205:853–868. [PubMed: 18362175]
26. Depoil D, Fleire S, Treanor BL, Weber M, Harwood NE, Marchbank KL, Tybulewicz VL, Batista FD. CD19 is essential for B cell activation by promoting B cell receptor-antigen microcluster formation in response to membrane-bound ligand. Nat Immunol. 2008; 9:63–72. [PubMed: 18059271]
27. Carrasco YR, Fleire SJ, Cameron T, Dustin ML, Batista FD. LFA-1/ICAM-1 interaction lowers the threshold of B cell activation by facilitating B cell adhesion and synapse formation. Immunity. 2004; 20:589–599. [PubMed: 15142527]
28. Thyagarajan R, Arunkumar N, Song W. Polyvalent antigens stabilize B cell antigen receptor surface signaling microdomains. J Immunol. 2003; 170:6099–6106. [PubMed: 12794139]
29. Fleire SJ, Goldman JP, Carrasco YR, Weber M, Bray D, Batista FD. B cell ligand discrimination through a spreading and contraction response. Science. 2006; 312:738–741. [PubMed: 16675699]
30. Arana E, Vehlow A, Harwood NE, Vigorito E, Henderson R, Turner M, Tybulewicz VL, Batista FD. Activation of the small GTPase Rac2 via the B cell receptor regulates B cell adhesion and immunological-synapse formation. Immunity. 2008; 28:88–99. [PubMed: 18191593]
31. Harwood NE, Batista FD. The cytoskeleton coordinates the early events of B-cell activation. Cold Spring Harb Perspect Biol. 2011; 3
32. Gabbiani G, Chaponnier C, Zumbe A, Vassalli P. Actin and tubulin co-cap with surface immunoglobulins in mouse B lymphocytes. Nature. 1977; 269:697–698. [PubMed: 413049]
33. Braun J, Hochman PS, Unanue ER. Ligand-induced association of surface immunoglobulin with the detergent-insoluble cytoskeletal matrix of the B lymphocyte. J Immunol. 1982; 128:1198–1204. [PubMed: 6976988]
34. Schreiner GF, Fujiwara K, Pollard TD, Unanue ER. Redistribution of myosin accompanying capping of surface Ig. J Exp Med. 1977; 145:1393–1398. [PubMed: 323408]
35. Braun J, Fujiwara K, Pollard TD, Unanue ER. Two distinct mechanisms for redistribution of lymphocyte surface macromolecules. I. Relationship to cytoplasmic myosin. J Cell Biol. 1978; 79:409–418. [PubMed: 309887]
36. Baeker TR, Simons ER, Rothstein TL. Cytochalasin induces an increase in cytosolic free calcium in murine B lymphocytes. J Immunol. 1987; 138:2691–2697. [PubMed: 3494083]
37. Brown BK, Song W. The actin cytoskeleton is required for the trafficking of the B cell antigen receptor to the late endosomes. Traffic. 2001; 2:414–427. [PubMed: 11389769]
38. Hao S, August A. Actin depolymerization transduces the strength of B-cell receptor stimulation. Mol Biol Cell. 2005; 16:2275–2284. [PubMed: 15728723]
39. Treanor B, Depoil D, Gonzalez-Granja A, Barral P, Weber M, Dushek O, Bruckbauer A, Batista FD. The membrane skeleton controls diffusion dynamics and signaling through the B cell receptor. Immunity. 2010; 32:187–199. [PubMed: 20171124]
40. Treanor B, Depoil D, Bruckbauer A, Batista FD. Dynamic cortical actin remodeling by ERM proteins controls BCR microcluster organization and integrity. J Exp Med. 2011; 208:1055–1068. [PubMed: 21482698]
41. Treanor B, Batista FD. Organisation and dynamics of antigen receptors: implications for lymphocyte signalling. Curr Opin Immunol. 2010; 22:299–307. [PubMed: 20434893]
42. Sharma S, Orlowski G, Song W. Btk regulates B cell receptor-mediated antigen processing and presentation by controlling actin cytoskeleton dynamics in B cells. J Immunol. 2009; 182:329–339. [PubMed: 19109164]
43. Liu C, Miller H, Hui KL, Grooman B, Bolland S, Upadhyaya A, Song W. A balance of Bruton's tyrosine kinase and SHIP activation regulates B cell receptor cluster formation by controlling actin remodeling. J Immunol. 2011; 187:230–239. [PubMed: 21622861]
44. Peluso P, Wilson DS, Do D, Tran H, Venkatasubbaiah M, Quincy D, Heidecker B, Poindexter K, Tolani N, Phelan M, Witte K, Jung LS, Wagner P, Nock S. Optimizing antibody immobilization strategies for the construction of protein microarrays. Anal Biochem. 2003; 312:113–124. [PubMed: 12531195]

45. Grakoui A, Bromley SK, Sumen C, Davis MM, Shaw AS, Allen PM, Dustin ML. The immunological synapse: a molecular machine controlling T cell activation. Science. 1999; 285:221–227. [PubMed: 10398592]
46. Manders EMM, Verbeek FJ, Aten JA. Measurement of co-localization of object in dual-colour confocal images. J Microscopy. 1993; 169:375–382.
47. Chan AY, Raft S, Bailly M, Wyckoff JB, Segall JE, Condeelis JS. EGF stimulates an increase in actin nucleation and filament number at the leading edge of the lamellipod in mammary adenocarcinoma cells. J Cell Sci. 1998; 111(Pt 2):199–211. [PubMed: 9405304]
48. Van Troys M, Huyck L, Leyman S, Dhaese S, Vandekerkhove J, Ampe C. Ins and outs of ADF/cofilin activity and regulation. Eur J Cell Biol. 2008; 87:649–667. [PubMed: 18499298]
49. McGough AM, Staiger CJ, Min JK, Simonetti KD. The gelsolin family of actin regulatory proteins: modular structures, versatile functions. FEBS Lett. 2003; 552:75–81. [PubMed: 14527663]
50. Huang TY, DerMardirossian C, Bokoch GM. Cofilin phosphatases and regulation of actin dynamics. Curr Opin Cell Biol. 2006; 18:26–31. [PubMed: 16337782]
51. Spector I, Shochet NR, Kashman Y, Groweiss A. Latrunculins: novel marine toxins that disrupt microfilament organization in cultured cells. Science. 1983; 219:493–495. [PubMed: 6681676]
52. Bubb MR, Senderowicz AM, Sausville EA, Duncan KL, Korn ED. Jasplakinolide, a cytotoxic natural product, induces actin polymerization and competitively inhibits the binding of phalloidin to F-actin. J Biol Chem. 1994; 269:14869–14871. [PubMed: 8195116]
53. Freeman SA, Lei V, Dang-Lawson M, Mizuno K, Roskelley CD, Gold MR. Cofilin-Mediated F-Actin Severing Is Regulated by the Rap GTPase and Controls the Cytoskeletal Dynamics That Drive Lymphocyte Spreading and BCR Microcluster Formation. J Immunol. 2011; 187:5887–5900. [PubMed: 22068232]
54. Silacci P, Mazzolai L, Gauci C, Stergiopulos N, Yin HL, Hayoz D. Gelsolin superfamily proteins: key regulators of cellular functions. Cell Mol Life Sci. 2004; 61:2614–2623. [PubMed: 15526166]
55. Bernstein BW, Bamburg JR. ADF/cofilin: a functional node in cell biology. Trends Cell Biol. 20:187–195. [PubMed: 20133134]

Abbreviations

AF	Alexa Fluro
Btk	Bruton's tyrosine kinase
FI	fluorescence intensity
IRM	interference reflection microscopy
mAg	membrane associated antigen
MFI	mean fluorescence intensity
p-Cofilin	phosphorylated cofilin
pY	phosphotyrosine
sAg	soluble antigen
SHIP-1	SH2-containing inositol-5 phosphatase-1
Tf	transferrin
TFI	total fluorescence intensity
TIRFm	total internalization reflection microscopy
WASP	Wiscott Aldrich symptom protein

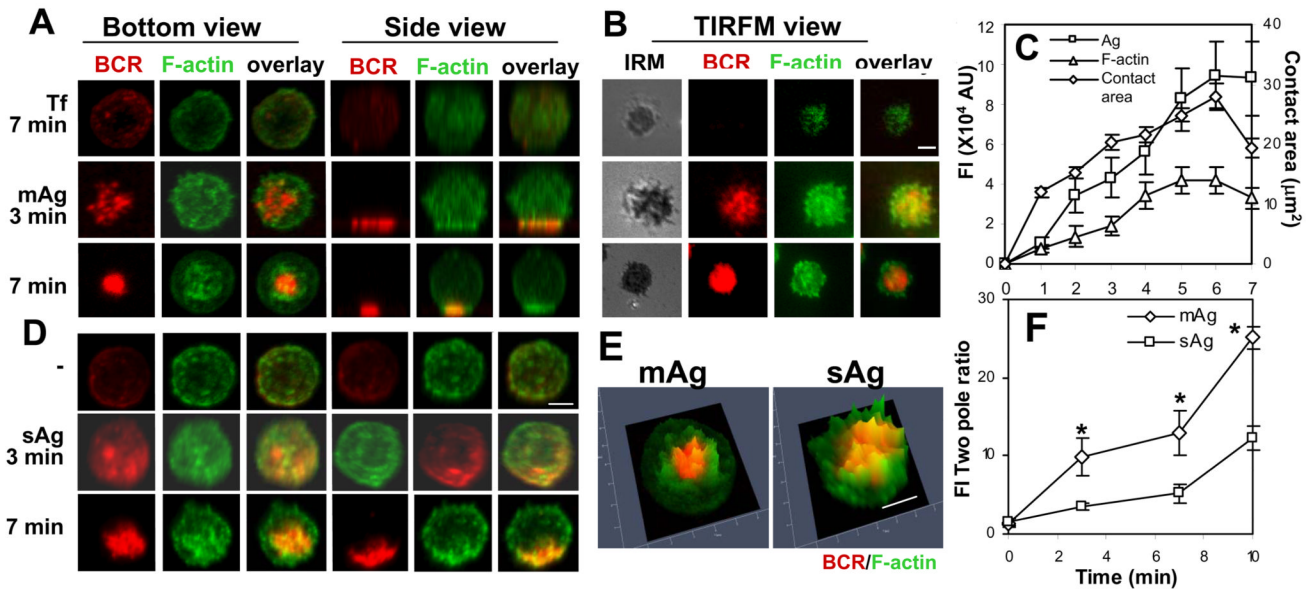

Figure 1.

The recruitment of F-actin to BCR aggregates in B-cells stimulated by membrane associated or soluble antigen. (A-C) To mimic mAg, splenic B-cells were incubated with AF546-mB-Fab′-anti-Ig tethered to lipid bilayers at 37°C for varying lengths of time. As controls, splenic B-cells were labeled with AF546-Fab-anti-Ig for the BCR before incubation with biotinylated transferrin (Tf)-tethered lipid bilayers. (D) To mimic sAg, splenic B-cells were incubated with AF546-mB-Fab′-anti-Ig for 10 min at 37°C to label the BCR. Then the cells were either incubated with streptavidin or with the medium alone (- or 0 min) as a control at 37°C for varying lengths of time. After fixation and permeabilization, the cells were stained for F-actin by AF488-phalloidin and analyzed using CFM. Series of Z-section images were acquired and reconstituted into 3-D images (A and D). The B-cell membrane contacting lipid bilayers was analyzed using TIRFM (B). The B-cell contact area and the total fluorescence intensity (TFI) of mAg and F-actin in the contact zone were quantified using Andor iQ software, and the data were plotted versus time (C). The distribution of F-actin in relation to BCR central clusters in B-cells stimulated with sAg and mAg for 7 min was analyzed by Zen software and is shown as 2.5-D fluorescence intensity profile (E), where yellow indicates colocalization. The fluorescence intensity ratios of F-actin at the BCR central cluster and at the opposite pole of the BCR central cluster (FI two pole ratio) in mAg- or sAg-stimulated B-cells were quantified using Andor iQ software (F). Shown are representative images and average values (±SD) from ~50 cells of three or four independent experiments. Scale bars, 2.5 μm. * $p<0.01$ compared to sAg in F.

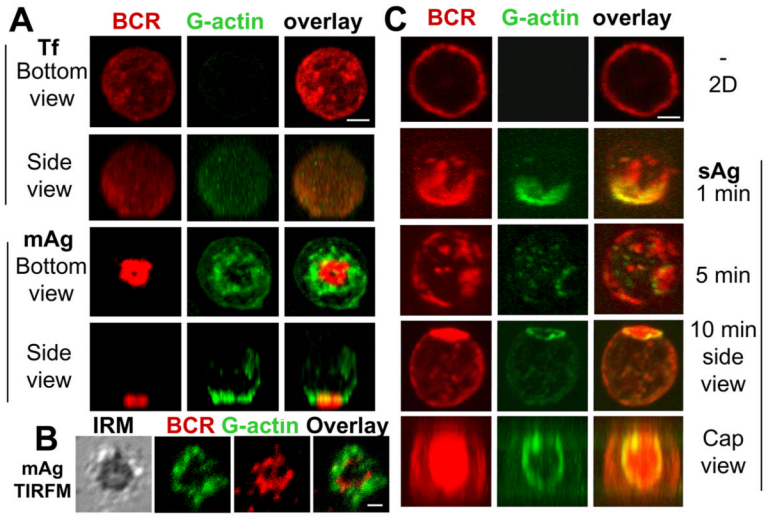

Figure 2.

Both membrane-associated and soluble antigens trigger actin polymerization at BCR aggregates. Splenic B-cells were incubated with AF546-mB-Fab′-anti-Ig tethered to lipid bilayers (mAg) in the presence of AF488-G-actin and 0.025% saponin at 37°C for 5 min, followed by fixation. 3-D images were acquired using a confocal microscope (A). The B-cell contact zone was imaged using TIRFM (B). Splenic B-cells were incubated with AF546-mB-Fab′-anti-Ig for 10 min and continued without (-) or with streptavidin (sAg) at 37°C for indicated times. In the last minute of the stimulation, cells were incubated with AF488-G-actin in the presence of 0.025% saponin. Cells were fixed and analyzed by CFM (C). Shown are representing 2-D, 3-D CFM and TIRFM images from three independent experiments. Scale bars, 2.5 μm.

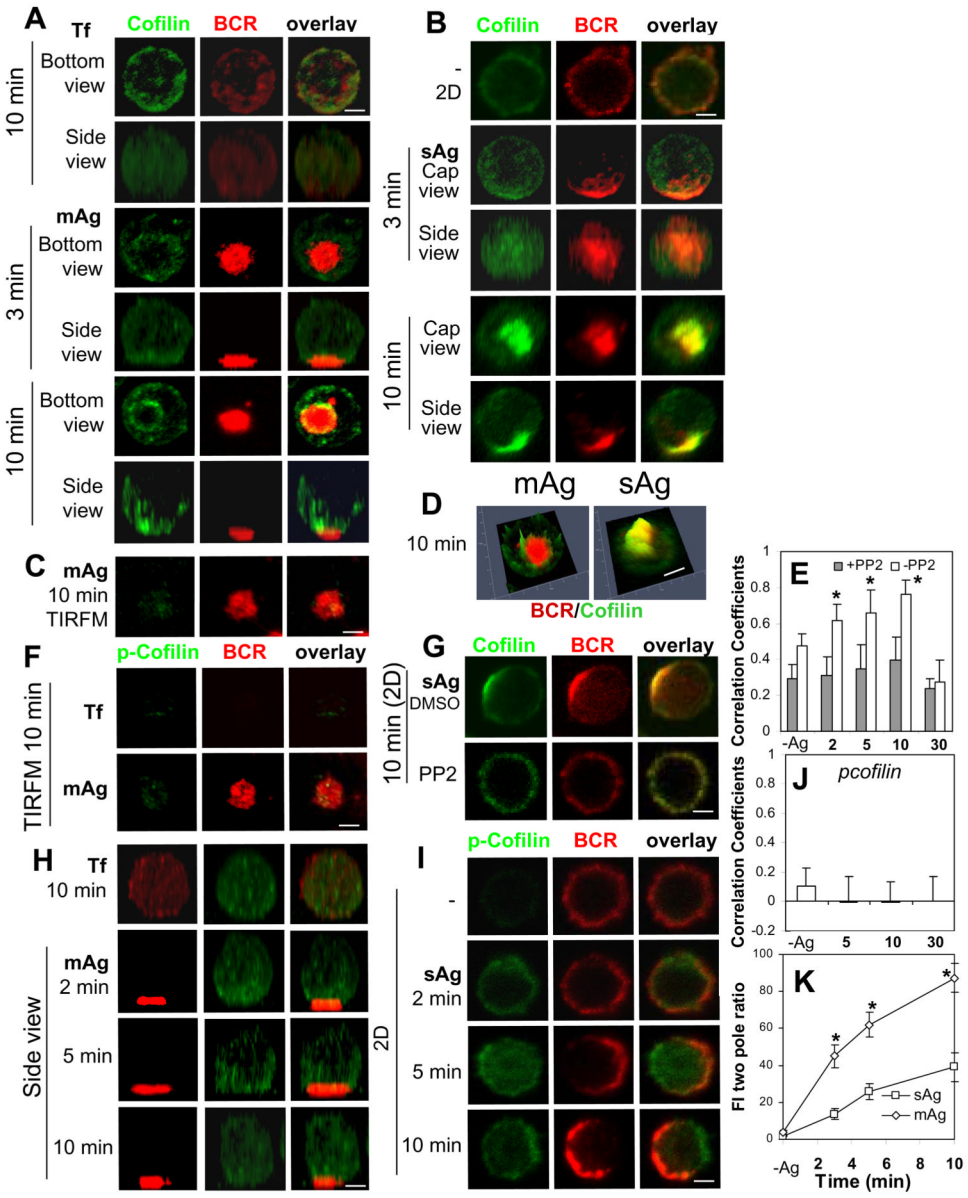

Figure 3.

Both membrane-associated and soluble antigens induce the recruitment of cofilin in a signaling-dependent manner. Splenic B-cells were incubated with AF546-mB-Fab′-anti-Ig tethered to lipid bilayers (mAg) at 37°C for indicated times. Cells were fixed, permeabilized, stained for cofilin (A and C) and phosphorylated cofilin (p-cofilin) (F and H), and analyzed by 3-D CFM (A and H) and TIRFM (C and F). Splenic B-cells pretreated without (B and I) or with PP2 (G) were incubated with AF546-mB-Fab′-anti-Ig without (-) or with streptavidin (sAg) at 4°C, washed, and warmed to 37°C for varying lengths of time. After fixation and permeabilization, the cells were stained for cofilin (B and G) or p-Cofilin (I), and analyzed using CFM. Fluorescence intensity profiles (2.5-D) of cofilin and BCRs in B-cells stimulated by mAg and sAg for 10 min were generated using Zen software (D). The Pearson's correlation coefficients between BCR and cofilin (E) or p-cofilin (J) staining were determined. The fluorescence intensity ratio of cofilin at the BCR central cluster to that at its opposite pole (FI two pole ratio) in B-cells stimulated by mAg and sAg was determined

using Andor iQ software (K). Shown are representative 2-D, 2.5-D, 3-D CFM and TIRFM images at indicated times and the average values (±SD) of ~50 cells from three independent experiments. Scale bars, 2.5 μm. * $p<0.01$ compared to PP2 treatment in E and compared to sAg in I.

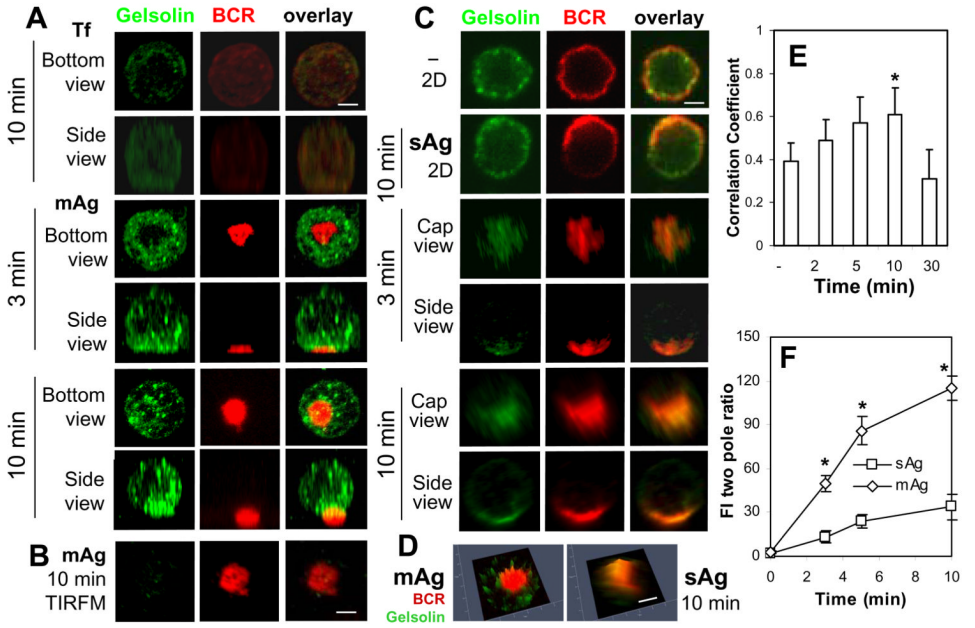

Figure 4.

The recruitment of gelsolin to BCR clusters in B-cells stimulated by soluble or membrane-associated Ag. Splenic B-cells were incubated with AF546-mB-Fab′-anti-Ig tethered to lipid bilayers (mAg) at 37°C for indicated times. Cells were fixed, permeabilized, stained for gelsolin, and analyzed by CFM (A) and by TIRFM (B). Splenic B-cells were incubated with AF546-mB-Fab′-anti-Ig without (-) or with streptavidin (sAg) at 4°C, washed, and warmed to 37°C for varying lengths of time. After fixation and permeabilization, the cells were stained for gelsolin and analyzed using CFM (C). The 2.5-D fluorescence intensity profiles of BCRs and gelsolin were generated using Zen software (D). The Pearson's correlation coefficients between BCR and gelsolin staining in sAg-stimulated cells were determined using Zen software (E). The two pole ratio of gelsolin fluorescence intensity was determined using Andor iQ software (F). Shown are representative 2-D, 2.5-D, and 3-D images at indicated times and the average values (±SD) of ~50 cells from three independent experiments. Scale bars, 2.5 μm. * $p<0.01$ compared to no streptavidin (-) in E and compared to sAg in F.

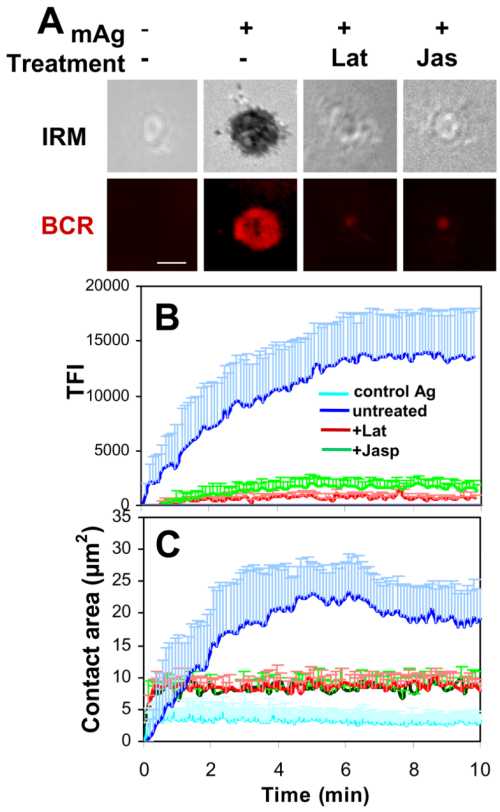

Figure 5.

Inhibition of actin reorganization blocks BCR aggregation and cell spreading in membrane-associated antigen-stimulated B-cells. Splenic B-cells were pretreated with or without latrunculin B (Lat, 10 μM) or jasplakinolide (Jas, 2 μM) for 30 min and then incubated with AF546-mB-Fab′-anti-Ig or non-specific antibody (Control Ag) tethered to lipid bilayers at 37°C. Time lapse images were acquired using TIRFM (A). The B-cell contact area (C) and the total fluorescence intensity (TFI) of AF546-mB-Fab′-anti-Ig in the contact zone (B) were quantified using Andor iQ software, and the data were plotted versus time. Shown are representative images of cells at 7 min (A) and the average contact area (C) and Ag TFI (+SD) (B) from ~ 20 cells of three independent experiments. Scale bars, 2.5 μm.

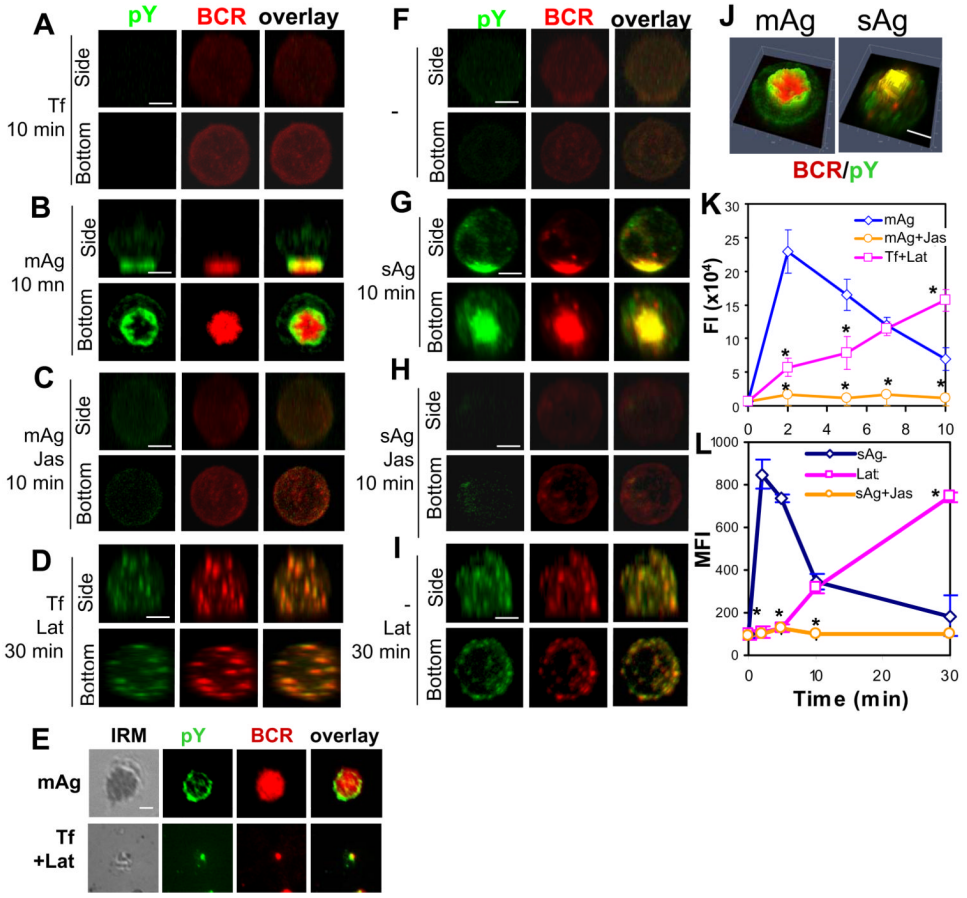

Figure 6.

Disruption of the actin cytoskeleton alters signal activation in response to both membrane-associated and soluble antigens and antigen-independent signal activation. For mAg stimulation, splenic B-cells that were pretreated without (B and E top panels) or with Jas (C) were incubated with AF546-mB-Fab′-anti-Ig tethered lipid bilayers at 37°C for indicated times. For a negative control of mAg, splenic B-cells were stained with AF546-Fab-anti-Ig first and then incubated with Tf-tethered lipid bilayer at 37°C for indicated times (A). For Lat treatment, B-cells labeled with AF546-Fab-anti-Ig were incubated with Lat and Tf-tethered lipid bilayer at the same time (D and E, bottom panels). For sAg stimulation, splenic B-cells that were pretreated without (G) or with Jas (H) were incubated with AF546-mB-Fab′-anti-IgG plus streptavidin at 37°C for indicated times. For a negative control of sAg, splenic B-cells were labeled with AF546-mB-Fab′-anti-Ig for the BCR first and then incubated with medium at 37°C for indicated times (F). For Lab treatment, B-cells labeled with AF546-mB-Fab′-anti-Ig were incubated with Lat (I). After fixation and permeabilization, the cells were stained for phosphotyrosine (pY) and analyzed using CFM (A-D and F-J) and TIRFM (E). Shown are representative 3-D CFM images (A-D and F-I), fluorescence intensity profiles (2.5-D) of pY and BCRs (J), and TIRFM images (E) from three independent experiments. Scale bars, 2.5 μm. The total fluorescence intensity of pY in individual cells stimulated by mAg was determined by summing the fluorescence intensity of all z-sections of a cell, and shown are the average fluorescence intensity (FI) (±SD) of ~50 cells from three individual experiments (K). The MFI of pY in sAg-stimulated cells was quantified using flow cytometry, and shown are the average MFI (±SD) of pY staining of

three independent experiments (L). * $p<0.01$ compared to cells treated with mAg (K) or sAg (L) without Lat or Jas.